Simulation of Wake Vortex Radiometric Detection via Jet Exhaust Proxy

Taumi S. Daniels

Electromagnetics and Sensors Branch, NASA Langley Research Center, Hampton, VA, 23681 USA

ABSTRACT

This paper describes an analysis of the potential of an airborne hyperspectral imaging IR instrument to infer wake vortices via turbine jet exhaust as a proxy. The goal was to determine the requirements for an imaging spectrometer or radiometer to effectively detect the exhaust plume, and by inference, the location of the wake vortices. The effort examines the gas spectroscopy of the various major constituents of turbine jet exhaust and their contributions to the modeled detectable radiance. Initially, a theoretical analysis of wake vortex proxy detection by thermal radiation was realized in a series of simulations. The first stage used the SLAB plume model to simulate turbine jet exhaust plume characteristics, including exhaust gas transport dynamics and concentrations. The second stage used these plume characteristics as input to the Line By Line Radiative Transfer Model (LBLRTM) to simulate responses from both an imaging IR hyperspectral spectrometer or radiometer. These numerical simulations generated thermal imagery that was compared with previously reported wake vortex temperature data. This research is a continuation of an effort to specify the requirements for an imaging IR spectrometer or radiometer to make wake vortex measurements. Results of the two-stage simulation will be reported, including instrument specifications for wake vortex thermal detection. These results will be compared with previously reported results for IR imaging spectrometer performance.

Keywords: radiometer, Fourier transform spectrometer, wake vortex, atmospheric modeling, numerical simulation

1. INTRODUCTION

Currently, there is no reliable commercially available airborne instrument capable of wake vortex detection in all weather conditions. Previous efforts have concentrated on active sensors, such as radar, to measure the velocity of hydrometeors. Most commercial aircraft are equipped with X-band Doppler radar. This system is designed to measure line of sight velocity relative to the sensing platform. However, this is a drawback as the rotation of the wake vortex flow is nearly perpendicular to the line of sight of an instrument on a following aircraft.

One potential solution is detection by a passive IR imaging Fourier transform spectrometer (FTS) or radiometer. In this context, a passive sensor is a receiver of electro-magnetic energy only, and in this application, the spectrum of interest is in the IR band from about 650 cm^{-1} to 3350 cm^{-1}. Throughout this paper, IR spectrum data is referred to in units of wavenumber (cm^{-1}) or inverse wavelength. An imaging FTS employs an array of photodetectors. If mounted on an aircraft in a forward looking configuration, an imaging IR hyperspectral FTS instrument could measure the high resolution temperature structure of the atmosphere ahead of the aircraft. This investigation applied knowledge of IR spectrometer or radiometer measurement performance based on jet exhaust entrained in wake vortices generated by an aircraft in varied atmospheric conditions as the determinant for discovering instrument requirements.

The IR FTS has shown promise in previous feasibility studies. In Gimmestad et al., the authors indicated that an airborne radiometer could be used to detect icing, volcanic ash, and turbulence, three of the main aviation hazards facing pilots.[1] A single instrument that can perform all of these measurements is very desirable. This research was continued with simulations of clear air turbulence, runway surface state, volcanic ash, icing, wind

Further author information:
E-mail: taumi.daniels@nasa.gov, Telephone: 757 864 4659

shear, and wake vortices and results of field deployments with two different IR FTS instruments.[2–4] Additional efforts to characterize imaging IR spectrometers to detect wake vortices was conducted.[5,6] In these studies, both long wave IR (LWIR, 700 to 1300 cm^{-1}), midwave IR (MWIR, 2000 to 3300 cm^{-1}) spectrometer bands were investigated. Both Fourier Transform Spectrometer and imaging IR radiometers were investigated, but only for the indirect thermal measurement of the atmosphere as a means of detecting the wake vortices. The target aircraft for this prior work was the Boeing B747, and will remain the same with this current effort. This research builds on previous efforts while exploring spectrometer requirements for this aviation hazard application.

The concept of an airborne spectrometer for remote detection of atmospheric species is not novel. Indeed, this type of instrument has been used to detect exhaust gases[7] and chemical signatures,[8] two of many examples. The interest for these prior researchers was for remote measurement of exhaust gas constituent concentrations, but not as a proxy for wake vortices. This prior work makes the current research more feasible in concept.

In this paper, initial results are presented along with particular imaging IR spectrometer or radiometer requirements. The next three sections include a brief review of relevant research, a description of how the SLAB[9] model was implemented to generate a jet exhaust plume, and an overview how the LBLRTM[10] model was used. The overall simulation attempts to examine jet engine exhaust as a tracer for wake vortex detection. The SLAB model computes exhaust gas concentrations and the LBLRTM model simulates spectrometer responses to the exhaust gases. The next section includes an analysis of the wake vortex thermal imagery results. The paper concludes with a discussion of results, a description of the indicated instrument requirements for wake vortex detection, and recommendations for future research.

2. PRIOR STUDIES

Of interest for this research was turbine engine exhaust interaction with wake vortices and the possibility of using this enhanced flow for wake vortex detection. A review of prior studies was conducted to determine turbine jet exhaust concentrations and temperatures. The time duration and strength of the vortices as well as their approximate physical structure was of interest for these simulations.

As noted in Gerz et al., during the cruise phase of flight, the exhaust jet diffused quickly with ambient air creating a turbulent region of flow with elevated temperature.[11] Some of this exhaust was then wound around each vortex, creating a warmer cylinder around a cooler core. Jet engine wing location relative to the wingtip has an impact on the extent of mixing. The outer engine location, relative to the wingtip for a Boeing B747 four-engine commercial aircraft, is estimated as 30 percent of wing span from the wingtip.[12] Wing span is the distance between the wing tips. In comparison, a similar estimate was made for a Boeing B777 using wing span information.[13] For this two-engine aircraft configuration, the engines are located at 60 percent of wing span from the wingtips. Mature vortices were reported by Gerz et al. to be located at about 11 percent of span from the wingtips, so four-engine configurations are more likely to have pronounced wake vortex engine jet interactions.[11]

Schilling et al. simulated exhaust dispersion for the Boeing B747 case.[14] They found that the outer jet engines' exhaust was entirely entrained within the wake vortices. In addition, they found that the inner engines produced exhaust that wrapped around the vortices at a much larger radius. Regarding the time duration, the authors found that this combined system of entrained exhaust was fully formed at 30 s and remained intact up to 120 s after initiation.

In a study of the effect of wake vortices on the entrainment and diffusion rate of exhaust gases, Garnier et al, used a numerical model for a Boeing B747 up to 30 s after initiation.[15] Their results were compared with measured data and showed good agreement for axial tracer concentrations. They found that turbulence had less of an effect on the entrainment process in the near field (up to 30 s after initiation). Their results indicate that a simple plume model for the jet exhaust can be used in the near field.

Curtius et al. reported measured temperature differences across vortex cores ranging from 0.8 to 1.4 °C for distances behind the generating aircraft ranging from 400 to 800 m.[16] These results were for an VFW-Fokker 614 aircraft,[17] one-third the wing span and 1/20 the maximum takeoff weight of a Boeing B747.[12] The Fokker aircraft was powered by two Rolls-Royce/Snecma M45H turbines, with about 8 times less thrust than the typical B747 turbine. Although an underestimate, the 0.8 to 1.4 °C temperature range (and distance) was used as a basis in this research for the exhaust gases entrained within the wake vortices.

Table 1: SLAB Parameters

Parameter	Value	Parameter	Value
Source Type	Horizontal Jet	Relative Humidity	15 %
Source Duration	600 s	Source Temperature	580 K
Source Area	0.8 m^2	Surface Roughness Height	30 m
Averaging Time	1 s	Downwind Distance	2000 m
Wind Speed	8 m/s	Ambient Temperature	269 K

Gago et al. found that a mature wake vortex was found to survive after entrainment of jet exhaust in a numerical model simulation.[18] The authors performed a temporal direct numerical simulation of a heated jet mixing with three-dimensional turbulence and a wake vortex. Their results illustrated that vortex core temperature does not change after jet exhaust entrainment. The exhaust gas was rolled up around the core and as a result, dissipated more quickly. The model simulation did not include IR active gases such as H_2O and CO_2.

With regard to the time duration of the wake vortices, Rahm et al. reported values of normalized circulation versus normalized time based on data from an airborne lidar.[19] The authors found that circulation strength dissipated by two-thirds after a time of about 30 s. Note that vortex decay time is strongly influenced by the level of ambient turbulence. The time period of interest extends while the vortices have circulation strength greater than 150 m^2/s (or about one third of the lower bound of the Boeing B747 initial circulation strength). Note that the initial circulation strength was reported by Nelson et al. in the range of 400 to 600 m^2/s.[20]

A summary of jet exhaust entrainment in vortices includes these key features determined from prior research: vortex core has elevated temperature up to 1.4 °C; vortices remain intact with significant circulation strength up to 120 s after initiation; a plume model can be used in the near-field; and light turbulence tends to increase vortex dissipation rate. The next question to resolve is the magnitude of the active IR gas concentrations within the entrained exhaust.

3. JET EXHAUST SIMULATION

The SLAB model was used for modeling turbine jet exhaust gas concentration. This model computes concentrations of a gas as it disperses in the atmosphere. Among four different source modes, the one used for this research was horizontal jet. The resulting plume is the time-averaged concentration depending on various input parameters that specify the atmosphere and the selected gas. A similar approach to modeling exhaust dispersion and entrainment within wake vortices used a box model and associated gas concentration profiles.[23] For this research, the SLAB model was executed several times for varied altitudes to match the spectrometer as observer altitude. In Section 2, a review of the scientific literature suggested that wake vortex detection using jet exhaust gas as a proxy was possible. This section describes a modeling effort to simulate concentrations of jet engine exhaust gases entrained within a wake vortex.

Specific exhaust gas constituents were determined from the jet fuel combustion reaction. Jet fuel was represented as dodecane, with molecular formula $C_{12}H_{26}$. As reported in Spicer et al., incomplete combustion and high reaction temperatures result in many products including numerous hydrocarbon fraction components as well as NO_X gases.[24] For this research, jet exhaust was modeled using the following incomplete combustion reaction: $C_{12}H_{26} + N_2 + 15O_2 \; ! \;\; 2C + 2CO + 7CO_2 + NO + NO_2 + CH_4 + 11H_2O$. Next, the molar ratios of the various exhaust products were estimated based on measured concentrations of CO_2. Black carbon (soot), though in the equation, and SO_2 are products of jet fuel combustion that were not included in this research. These two products are intended to be examined in future research. The next step is to determine atmospheric gas concentrations of the other products.

Gas concentrations were determined using the following steps: use research literature to estimate Boeing B747 fuel consumption rates, derive a dodecane combustion rate, then use stoichiometric ratios from the incomplete combustion equation to compute gas product source concentrations at the jet nozzle. These values are then used as inputs to the SLAB model for mass flow rate at the jet nozzle for each different gas. Knowing the approximate concentration at the source, the SLAB output is then used to create an atmospheric model containing the jet

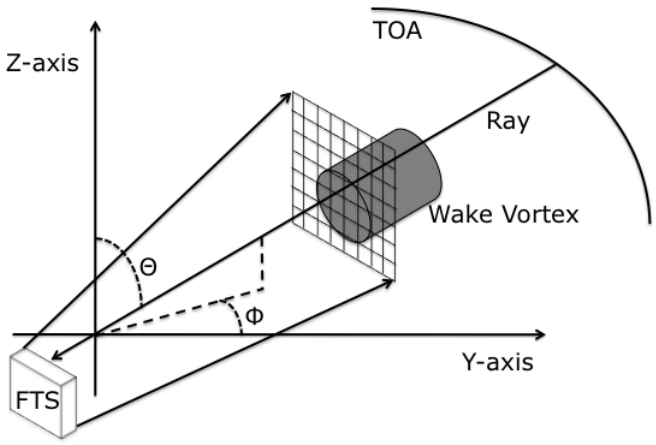

Figure 1: Geometry for FTS Simulations. A typical ray is shown penetrating a wake vortex, extending from the top of the atmosphere to a FTS mounted on an aircraft.

exhaust plume with each gas constituent spatial concentration. This plume is then embedded in an atmosphere that is then used as input to LBLRTM.

At a General Electric jet engine facility, [CO_2] was measured directly behind a CFM-56 turbine engine.[24] In particular, gas concentrations from their results were interpolated to yield [CO_2] = 3.16 □ 10^4 ppmv for a fuel flow of 1424.28 kg/hr. This particular fuel flow compared favorably with the reported value from Schulte et al.[25] Data were selected from a ground-based study and an in-situ flight study. In both studies, a nondispersive infrared sensor was used to measure [CO_2] in CFM-56 turbine jet engine exhaust. This particular turbine jet engine is often used on Boeing B747 aircraft.

For all SLAB runs, the following parameters for each gas were input to the model: molecular weight, vapor heat capacity, boiling temperature, heat of vaporization, liquid heat capacity, liquid density, and liquid mass fraction. In addition, other SLAB input parameters include the horizontal jet height, mass source rate, and atmospheric conditions listed in Table 1. The molar ratio in the incomplete combustion reaction determined the mass source for each gas which then remained constant for that gas and for any changes in observer altitude.

Using the steps listed above, the jet exhaust plume gases had the following source concentrations: [H_2O] 5177 ppm, [CO_2] 3295 ppm, [CO] 941 ppm, [CH_4] 471 ppm, [NO_2] 471 ppm, and [NO] 471 ppm. Each of these concentrations are consistent with measured values reported in the literature,[26].[27] These values were input to SLAB in separate runs to compute plume concentrations. This model simulates the dispersion of gases as a Gaussian plume in the atmosphere. SLAB only models one gas species as a plume in the atmosphere at a time, and as such, was computed separately for each exhaust gas constituent. All of the separate SLAB runs for each gas were then combined into a single jet exhaust plume. Measured concentrations of exhaust gas constituents compare well with this estimated plume.[28, 29]

In this research, the exhaust plume is assumed to be completely entrained in the wake vortex. The second inner exhaust plume that would normally wind around the entrained outer exhaust plume is not modeled. Further, the exhaust plume composed of all the separate gases is used to estimate the gas concentrations in the near field region. In this idealistic scenario, turbulence is not modeled. Indeed, turbulence tends to increase dissipation of the vortices - making them less of an aviation hazard. Also, no cross winds nor shear winds are modeled. Again, these flows only tend to disrupt the vortices. The result of these assumptions is a worst-case scenario in terms of aviation hazard, but an idealized best-case for spectrometer detection. The next section describes the spectrometer modeling process.

Table 2: Overall LBLRTM simulation parameters

Type	Parameter	Range or Value
Aircraft	Altitude (km)	0, 1, 3, 6 and 10
FTS	LWIR Band (cm^{-1})	870 - 1330
FTS	MWIR Band (cm^{-1})	2000 - 3330
FTS	Spectral Resolution (cm^{-1})	0.5 (unapodized)
FTS	Image Pixel Array	26 by 26
FTS	Elevation Angle (degrees)	5
Wake Vortex	Separation Distance (km)	0.5
Wake Vortex	Wake Vortex Depth (km)	0.3

4. SPECTROMETER SIMULATION

The LBLRTM, described by Clough et al., is a highly configurable model for the computation of radiant flux in the atmosphere.[30,31] The user supplies an atmospheric description including gas concentrations and pressure levels. The model assumes a plane parallel atmosphere of multiple layers with radiance estimated along any specified ray defined by zenith angle Θ and azimuth angle Φ, as shown in Figure 1. The output of the LBLRTM is radiance, in units $W/cm^2/sr/cm^{-1}$. The term "FTS" is used here but could also refer to a radiometer of similar capability.

For this research, the LBLRTM was used as the basis for simulation of an imaging IR FTS. An FTS image consists of an array of pixels. Each pixel was simulated as a single ray through the atmosphere. This radiative model requires a monotonically increasing atmosphere, a constraint that imposes an upward looking geometry. As shown in Figure 1, an example optical ray originates at the top of atmosphere (TOA) and extends through the wake vortex (wake vortex length was 300 m) to an upward looking IR FTS instrument on the ground or mounted on a following aircraft (at 500 m from the vortex). The geometry was the same for changes in altitude for the aircraft mounted cases. The figure depicts an array of pixels, although for this research, only a subset of pixels across the vortex are required. The question is how much temperature or gas concentration difference can be detected by a spectrometer.

A ray, or collection of points on a line, was used as input to the LBLRTM. This model solves the radiative transfer equation based on atmospheric state specifications. The result was a spectrum of radiance estimates for each pixel over a specified IR band. As each pixel of the two-dimensional image had an associated IR spectrum, the collection of all image spectra formed a three-dimensional FTS data cube. Atmospheric thermal variations between the FTS and the wake vortex were not simulated. The rays were chosen to penetrate that a portion of the entrained wake vortex region. Each point along a ray was defined by Z-axis height, zenith angle relative to local vertical, and temperature and jet exhaust gas concentrations embedded in the U.S. Standard Atmosphere.[32]

The HITRAN database includes spectroscopic parameters used by LBLRTM for each atmospheric gas at each wave number.[33] A subset of this database was created using an LBLRTM associated program called Line File (LNFL). This code extracted the gas parameters from the HITRAN database and performed various corrections, including those for temperature, pressure, and line coupling. The subset of gas parameters was then used as input to LBLRTM. Both of these computer programs and the HITRAN database were retrieved online.[10] The FORTRAN source codes were compiled using GNU Fortran Compiler (GCC) version 4.9.0.

Single pixels from a theoretical FTS were simulated using the parameters listed in Table 2. The spectral range of wave numbers used for all LBLRTM runs was 650 cm^{-1} to 3330 cm^{-1} encompassing the LWIR and MWIR ranges. Also, for all runs, the unapodized spectral resolution was 0.5 cm^{-1}. Several runs were performed using only a subsample of the total spatial image extent. The goal is to examine the temperature and gas constituent differences between jet exhaust and non-jet exhaust pixels.

The LBLRTM model has the user settable feature of selecting particular atmospheric gases and their respective concentrations. The selected gases included: H_2O, CO_2, CO, NO_2, NO, and CH_4. The SLAB data fields were spatially interpolated into the Standard Atmosphere at the desired altitude. Also, all FTS simulations were computed in the absence of clouds, aerosols, or any thermal sounding variations.

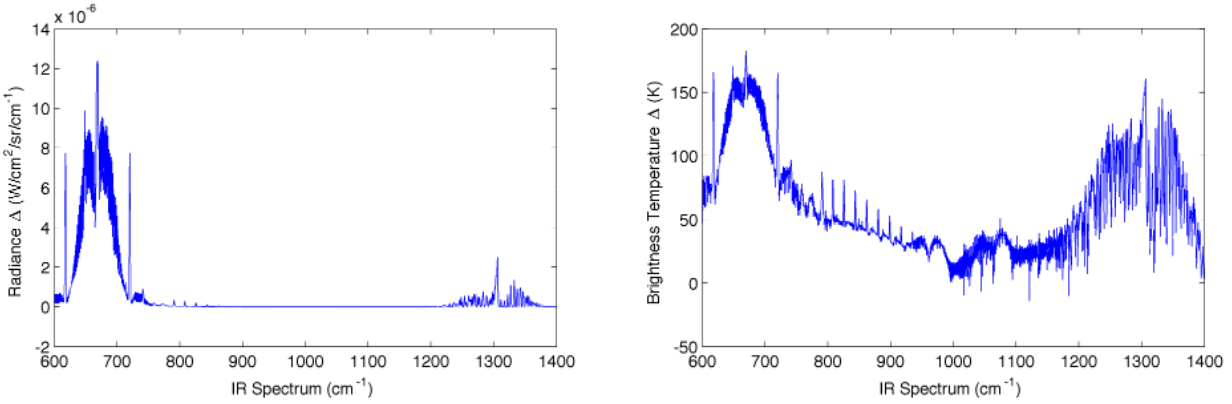

(a) (b)

Figure 2: Plots of radiance (a) and brightness temperature (b) emission spectrum differences over the LWIR band 600 cm^{-1} to 1400 cm^{-1} at altitude 3 km and 5 degree elevation.

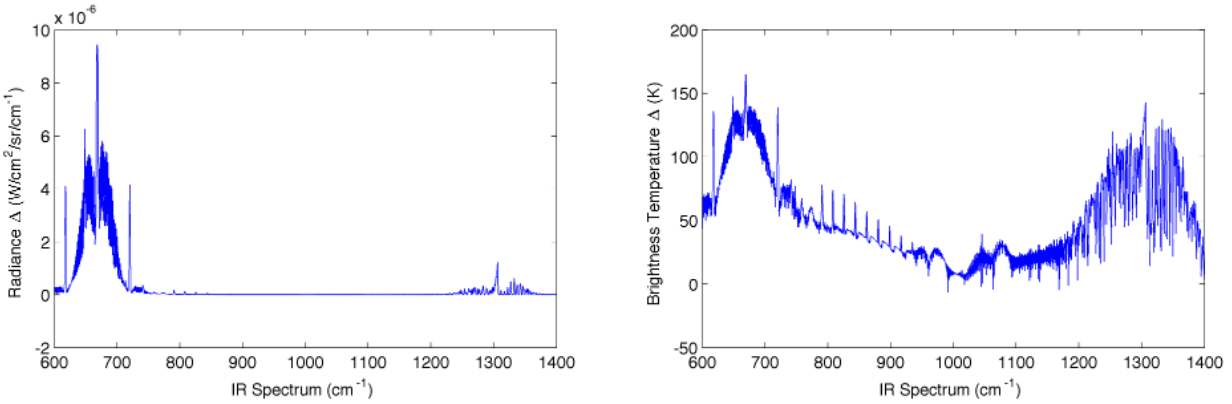

(a) (b)

Figure 3: Plots of radiance (a) and brightness temperature (b) emission spectrum differences over the LWIR band 600 cm^{-1} to 1400 cm^{-1} at altitude 6 km and 5 degree elevation.

LBLRTM rays extend from the TOA at about 100 km down to the spectrometer observer altitude. However, the SLAB vortex data were computed for a specific initial altitude descending over time. In order to perform the simulation at higher altitudes, temperature and exhaust gas concentrations were adjusted to be consistent with corresponding values of the U.S. Standard Atmosphere at the specified pressure altitude. Time after passage of the aircraft was modeled as decreases in temperature and in exhaust gas concentrations as the exhaust plume spread and diffused. The elevation angle $\Theta = 5$ degrees was selected assuming the geometry of two aircraft cruising at different altitudes. A higher leading-aircraft will generate vortices that descend into the path of the following aircraft. This geometry was assumed for all simulations at all altitudes.

Finally, as with all simulations, some compromises were necessary. The LBLRTM output was restricted to radiance along each azimuth ray. Surface emission and upwelling radiance were not considered. Direct solar radiation was not considered although the LBLRTM can model the sun at some azimuth and elevation relative to the point of view. Also, modeling multiple rays per array pixel was excluded because it exceeded the acceptable computational time threshold. Neither atmospheric scattering effects nor atmospheric hydrometeors were included in the model. Also, the modeled FTS is theoretical and does not include instrument responses (e.g. detector and/or noise response functions).

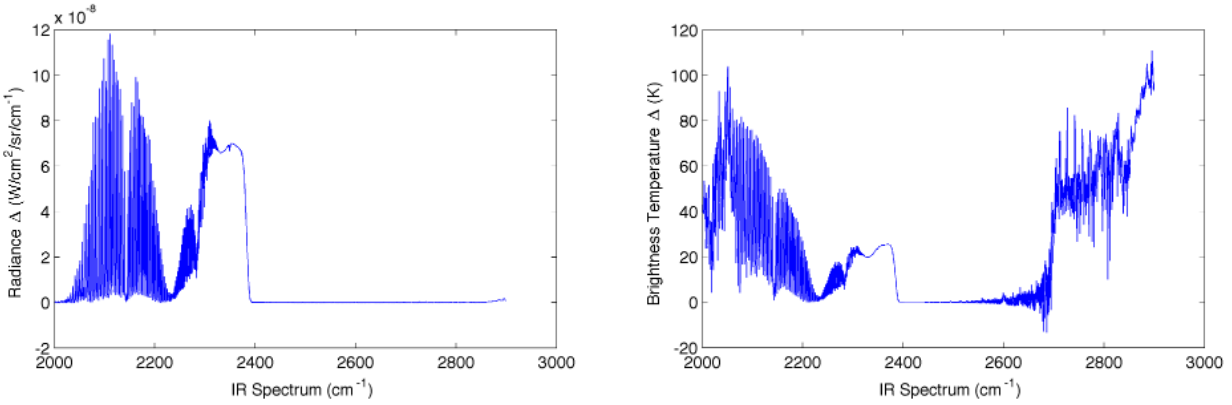

(a) (b)

Figure 4: Plots of radiance (a) and brightness temperature (b) emission spectrum differences over the MWIR band 2000 cm^{-1} to 2900 cm^{-1} at altitude 3 km and 5 degree elevation.

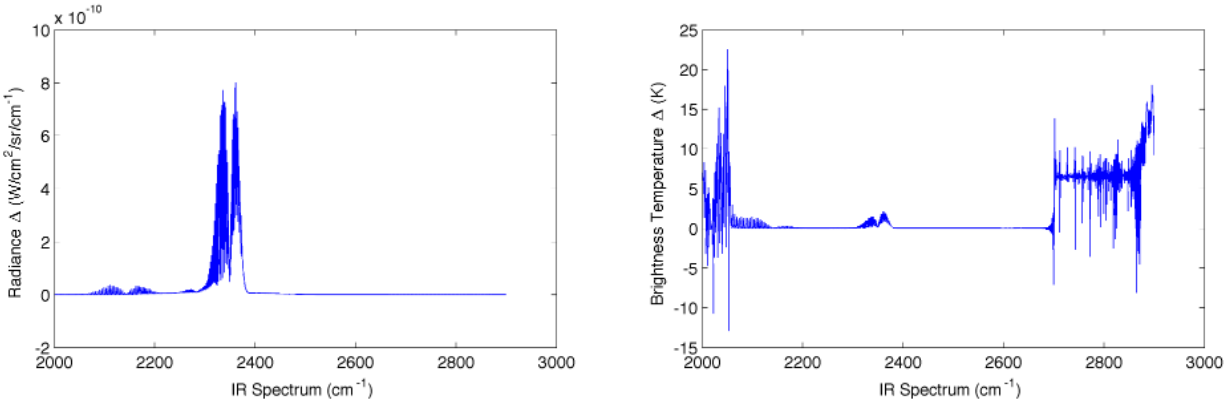

(a) (b)

Figure 5: Plots of radiance (a) and brightness temperature (b) emission spectrum differences over the MWIR band 2000 cm^{-1} to 2900 cm^{-1} at altitude 6 km and 5 degree elevation.

5. SIMULATION RESULTS

In a prior result, Daniels et al. found that an imaging IR FTS could detect wake vortices based on temperature differences.[5] However, for this to be achieved, the scene would necessarily need sufficient thermal contrast across pixels that encompassed the wake vortices. As a result, for this application, one major feature is the relative amplitude of the radiance difference across the IR spectrum. This radiance difference is the result of thermal differences across the IR spectrum due to the entrained jet exhaust compared to the ambient sky background. This feature enables a quick comparison of the radiance between just two pixels. Furthermore, the two pixels can be differenced to remove contributions to spectrum due to the background for a particular elevation and altitude viewing geometry. A series of plots of these differences are shown in subsequent figures. The pixel with the greatest levels of exhaust gas concentration is selected in each case.

Figure 2a is a plot of the radiance spectrum over the LWIR at the maximum radiance difference at an altitude of 3 km and an elevation of 5 degrees. The data in this plot is plotted as brightness temperature for the same IR band in Figure 2b. The brightness temperature plot illustrates more detail in the spectral difference, particularly in the 2700 cm^{-1} to 2900 cm^{-1} band. For this LWIR band, the active gases are CO_2, H_2O, N_2O, CH_4 and CO.

A similar pair of plots of the radiance spectrum over the LWIR are shown in Figure 3a and 3b. These plots show the result computed at altitude 6 km and elevation 5 degrees. As with the prior plots at 3 km, a comparison of radiance plot versus brightness temperature plot reveals the spectral detail due to water vapor at the each end of the LWIR band.

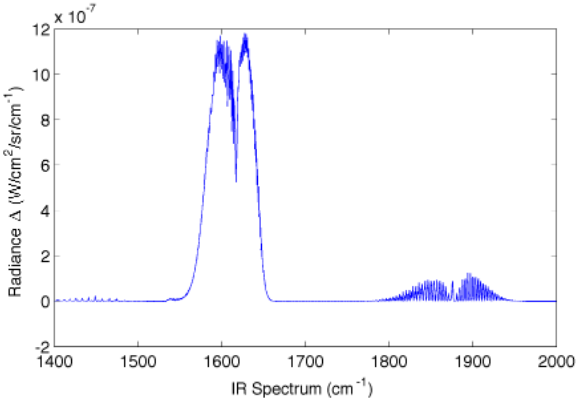

(a)

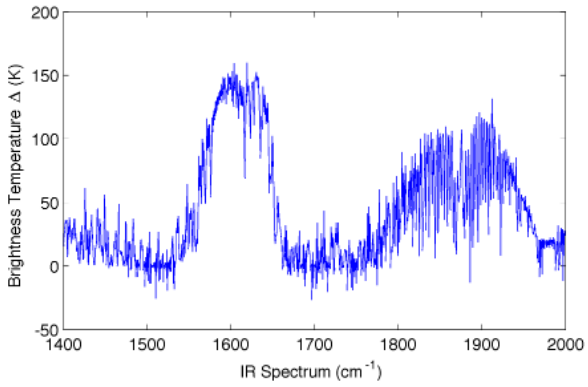

(b)

Figure 6: Plots of radiance (a) and brightness temperature (b) emission spectrum differences over the intermediate IR band 1400 cm^{-1} to 2000 cm^{-1} at altitude 3 km and 5 degree elevation.

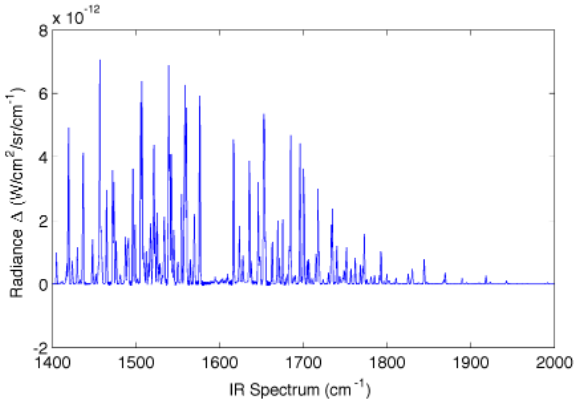

(a)

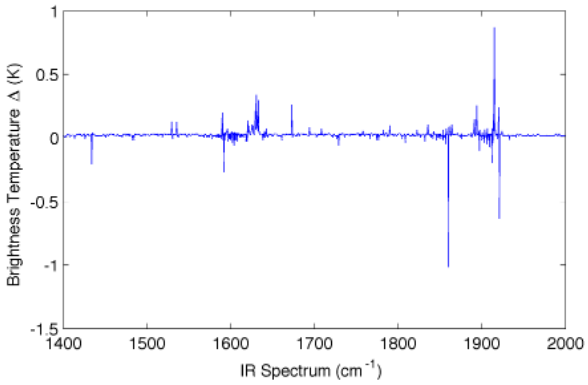

(b)

Figure 7: Plots of radiance (a) and brightness temperature (b) emission spectrum differences over the intermediate IR band 1400 cm^{-1} to 2000 cm^{-1} at altitude 6 km and 5 degree elevation.

A comparison of the two pairs of plots at 3 km versus 6 km altitude illustrate the impact of the decrease in IR absorption due to the decrease in overall emitted radiance at the higher altitude. The exhaust gas concentrations have not changed, however, the ambient temperature at the higher altitude has decreased. Along with this decrease in temperature is an increase in the cooling rate for the exhaust gas plume. As a result, note that the amplitude of the radiance differences has decreased by two orders of magnitude for only a change in 3 km in altitude. While these plots might indicate an adequate signal for using exhaust gas a proxy for the wake vortices at the lower altitude, the significant attenuation at the higher altitude places a greater requirement on the sensitivity of an on-board spectrometer.

A similar set of plot pairs is shown in the MWIR band in Figure 4a and Figure 4b at 3 km altitude, and Figure 5a and Figure 5b at 6 km altitude. These two pairs of plots are of the same two pixel differences and geometry as in the previous case except computed in the MWIR band. As before, a marked decrease in amplitude is evidenced by the extreme change in radiance amplitude (the plot in Figure 4a is 2 orders of magnitude greater than that of Figure 4a).

While current IR detectors are sensitive over specific spectral bands (MCT for LWIR vs InSb for MWIR), regardless of the detector technology, what IR thermal difference signal due to the jet exhaust is available in the intermediate IR band? To answer this question, a set of LBLRTM runs were performed over the intermediate IR spectral range from 1400 cm^{-1} to 2000 cm^{-1}.

The intermediate band was investigated for any potential thermal difference signal as shown in the Figure

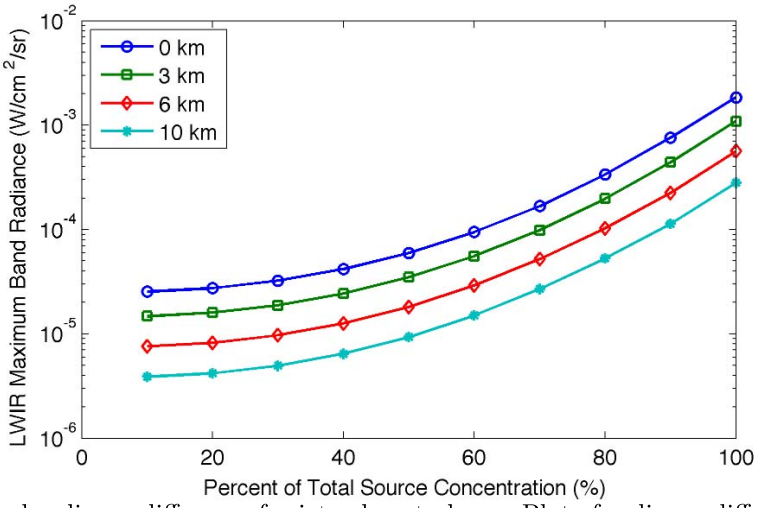

Figure 8: LWIR spectral radiance difference for jet exhaust plume. Plot of radiance difference emission spectrum integrated over the LWIR band versus exhaust gas as a percentage of maximum source concentration at different altitudes and 5 degree elevation.

6a and Figure 6b at 3 km altitude and Figure 7a and Figure 7b at 6 km altitude. As in the sets of plots for the other two IR bands, these figures reveal the various exhaust gas IR signatures. In particular, the CO_2 (large peak at about 1600 cm^{-1}) and H_2O (continuum centered around 1900 cm^{-1}) components can be seen in the plots. Unfortunately, the change in altitude from 3 km to 6 km results in a decrease in amplitude of 5 orders of magnitude.

An examination of the two pixel radiance differences in the intermediate IR band and a comparison to the levels computed for the LWIR and MWIR bands reveals the lack of a usable signal at 6 km altitude. This result precludes any consideration of using the intermediate IR band for this application.

Another downselect option is afforded by a comparison between the LWIR and MWIR brightness temperature differences. Specifically, the LWIR band spectral response is greater than that of the MWIR band. For this application, the entrained exhaust gases will, over time, lose their thermal contrast or difference with the background sky, effectively rendering the wake vortex undetectable by the spectrometer. As the LWIR band has a greater thermal difference, it is more desirable than the MWIR band.

A series of SLAB/LBLRTM runs were performed at different altitudes and source gas concentrations for the LWIR band. The exhaust gas at the source (jet nozzle) was varied from 0% to 100% as the altitude of the observing spectrometer was varied from 0 km to 10 km. The resulting two pixel difference spectra were integrated over the LWIR band. The integrated LWIR spectral radiances yielded a single value for each source gas exhaust concentration and at each altitude. The results of this series of SLAB/LBLRTM runs is shown in Figure 8.

The data in Figure 8 can be used to estimate the minimum spectrometer response required for this application under varying altitude conditions. For example, the change in integrated spectral radiance for an increase in source gas concentration from 20% to 30% is the difference in the computed radiance at these two levels, or 3.2x10^{-7} W/cm^2/sr. As the slopes of all four plots in the figure are approximately equal, this radiance difference appears to be altitude invariant. Using the data in this plot, similar minimum spectrometer signal levels can be estimated between different source gas concentrations for the LWIR band. Note however, that at a minimum, the spectrometer must be capable of detecting the signal level corresponding to a threshold minimum source gas concentration. For these estimate, a 20 % source gas concentration requires a corresponding detection level of 4.2x10^{-6} W/cm^2/sr.

In prior research, Daniels et al. reported a minimum signal level for an imaging radiometer to have a minimum brightness temperature sensitivity of 2 mK and a minimum spectral resolution of at least 16 cm^{-1}.[6] The authors

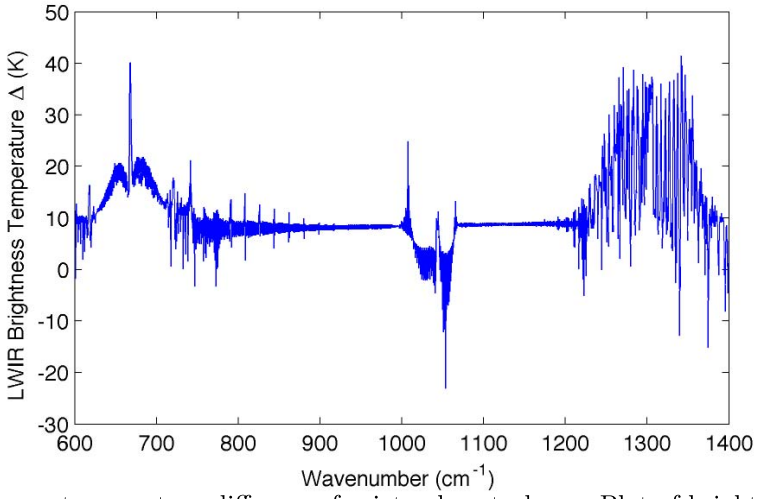

Figure 9: LWIR brightness temperature difference for jet exhaust plume. Plot of brightness temperature difference emission spectrum for the LWIR band and minimum exhaust gas source concentration at 10 km altitude and 5 degree elevation.

recommended five potential spectral bands, two of which match those determined in the current research. In particular, the 670 cm^{-1} to 750 cm^{-1} and 1250 cm^{-1} to 1450 cm^{-1} bands match those in the prior research and are again recommended based on exhaust gas as a proxy.

To estimate the minimum detectable brightness temperature requirement for an airborne spectrometer, the plot of the LWIR brightness temperature difference at atltitude 10 km, as shown in Figure 9, can be used. In the plot, the brightness temperature difference in the spectral band 670 cm^{-1} to 750 cm^{-1} has an amplitude of about 15 K. From this value, an extimate of the minimum detectable brightness temperature requirement can be set to 1/10 of this level, or 1.5 K. This is much greater than the estimate of 2 mK for the minimum spectrometer performance requirement as previously reported.[6]

6. CONCLUSION

Simulated wake vortices having realistic temperature and exhaust gas data were generated by means of the SLAB model. The combined single gas outputs of this model were used for the input atmosphere to the LBLRTM model. An imaging IR spectrometer instrument was simulated by means of the LBLRTM model, enabling investigation of the effects of temperature, water vapor, jet engine exhaust, distance, altitude, and elevation angle. A jet exhaust signal was revealed in the IR spectral data over two spectral bands, 670 cm^{-1} to 750 cm^{-1} and 1250 cm^{-1} to 1350 cm^{-1}. These two narrow IR bands correspond to CO_2 and H_2O, the two main chemical products of the incomplete combustion of jet fuel. For wake vortex detection using jet exhaust as a proxy, a recommended imaging radiometer should be sensitive within these LWIR spectral bands.

This recommended instrument must be capable of detecting a minimum radiance difference of at least $3.2x10^{-7}$ $W/cm^2/sr$. Assuming fully entrained jet exhaust within the modeled wake vortex, the recommended instrument detection performance is greater than the minimum spectral response that was previously reported.

In terms of radiance differences, modeled jet exhaust was found to be an enhancement or proxy for detecting wake vortices. Results with only modest increases in hydrocarbon combustion gas concentrations revealed much stronger exhaust spectral radiance signatures than mere temperature and absolute humidity changes due to vortices; however, the location of the jet engines relative to the wing tips becomes critical for exhaust gas rollup to occur. In the terminal area, a higher concentration of ambient exhaust gases would interfere with an exhaust gas based thermal detection scheme.

REFERENCES

[1] Gimmestad, G., Papanicolopoulos, C., Richards, M., Sherman, D., and West, L., "Feasibility Study of Radiometry for Airborne Detection of Aviation Hazards," Tech. Rep. CR-2001-210855, NASA (June 2001).

[2] West, L., Gimmestad, G., Smith, W., Kireev, S., Cornman, L., Schaffner, P., and Tsoucalas, G., "Applications of a Forward-Looking Interferometer for the On-board Detection of Aviation Weather Hazards," Tech. Rep. TP-2008-215536, NASA (October 2008).

[3] West, L., Gimmestad, G., Herkert, R., Smith, W., Kireev, S., Daniels, T., Cornman, L., Sharman, B., Weekley, A., Parram, G., Gross, K., Smith, G., Feltz, W., Taylor, J., and Olson, E., "Hazard Detection Analysis for a Forward-Looking Interferometer," in [1st AIAA Atmospheric and Space Environments Conference], (June 2009). AIAA 2009-3635.

[4] West, L., Gimmestad, G., Lane, S., Smith, B. L., Kireev, S., Daniels, T., Cornman, L., and Sharman, B., "Airborne Forward-Looking Interferometer for the Detection of Terminal-Area Hazards," Tech. Rep. CR-2014-218167, NASA (February 2014).

[5] Daniels, T., Smith, W., and Kireev, S., "Recent Developments on Airborne Forward Looking Interferometer for the Detection of Wake Vortices," in [4th AIAA Atmospheric and Space Environments Conference], (June 2012). AIAA 2012-2791.

[6] Daniels, T., Smith, W., and Kireev, S., "Simulation of Airborne Radiometric Detection of Wake Vortices," IEEE Transactions on Geoscience and Remote Sensing (2015). [In review, submitted 11/2014].

[7] Prel, F., Moreau, L., Lantagne, S., Roy, C., Vallières, C., and Leavesque, L., "MR-i: High-speed Dual-cameras Hyperspectral Imaging FTS," in [Proceedings of the SPIE, Electro-Optical Remote Sensing, Photonic Technologies and Applications V], Kamerman, G., ed., **8186** (2011).

[8] Tank, V., Haschberger, P., Lindermeir, E., and Matthern, K. H., "FTIR Airborne Measurement of Aircraft Jet Engine Exhaust Gas Emissions Under Cruise Conditions," in [Proceedings of the SPIE], **2506**, 359–367 (1995).

[9] Ermak, D. L., "User's Manual for SLAB: An Atmospheric Dispersion Model for Denser-than-Air Releases," tech. rep., Lawrence Livermore National Laboratory (June 1990). [Available online at http://www.epa.gov/ttn/scram/models/nonepa/slab.zip].

[10] Shephard, M., Cady-Pereira, K., and Rieu-Isaacs, H., "LBLRTM Version 12.0, LNFL Version 2.6, and Line Parameter Database Version 3.0. Atmospheric and Environmental Research," (2011).

[11] Gerz, T., Holzäpfel, F., and Darracq, D., "Commercial aircraft wake vortices," Progress in Aerospace Sciences **38**, 181–208 (April 2002).

[12] Boeing Company, "747 Airplane Characteristics," (2011). D6-58326. [Available online at http://www.boeing.com/commercial/airports/acaps/747_123sp.pdf].

[13] Boeing Company, "777 Airplane Characteristics," (May 2008). D6-58329. [Available online at http://www.boeing.com/commercial/airports/acaps/777_23.pdf].

[14] Schilling, V., Siano, S., and Etling, D., "Dispersion of aircraft emissions due to wake vortices in stratified shear flows: A two-dimensional numerical study," Journal of Geophysical Research: Atmospheres **101**(D15), 20965–20974 (1996).

[15] Garnier, F., Brunet, S., and Jacquin, L., "Modelling Exhaust Plume Mixing in the Near Field of an Aircraft," Annales Geophysicae **15**(11), 1468–1477 (1997).

[16] Curtius, J., Sierau, B., Arnold, F., Baumann, R., Busen, R., Schulte, P., and Schumann, U., "First Direct Sulfuric Acid Detection in the Exhaust Plume of a Jet Aircraft in Flight," Geophysical Research Letters **25**, 923–926 (Mar. 1998).

[17] German Aerospace Center, "VFW 614 ATTAS," (2008). [Available online at http://www.dlr.de/en/desktopdefault.aspx/tabid-4777/7916_read-11998/].

[18] Gago, C. F., Brunet, S., and Garnier, F., "Numerical Investigation of Turbulent Mixing in a Jet/Wake Vortex Interaction," AIAA Journal **45**(2), 2049–2061 (2002).

[19] Rahm, S. and Smalikho, I., "Aircraft Wake Vortex Measurement with Airborne Coherent Doppler Lidar," Journal of Aircraft **45**(4), 1148–1155 (2008).

[20] Nelson, R. C., "The Trailing Vortex Wake Hazard: Beyond the Takeoff and Landing Corridors," in [AIAA Atmospheric Flight Mechanics Conference and Exhibit], (August 2004).

[21] Shephard, M. W., Clough, S. A., Payne, V. H., Smith, W. L., Kireev, S., and Cady-Pereira, K. E., "Performance of the Line-by-Line Radiative Transfer Model (LBLRTM) for Temperature and Species Retrievals: IASI Case Studies from JAIVEx," Atmospheric Chemistry and Physics **9**(19), 7397–7417 (2009).

[22] Coheur, P.-F., Clarisse, L., Turquety, S., Hurtmans, D., and Clerbaux, C., "IASI Measurements of Reactive Trace Species in Biomass Burning Plumes," Atmospheric Chemistry and Physics Discussions **9**(2), 8757–8789 (2009).

[23] Kärcher, B., "A Trajectory Box Model for Aircraft Exhaust Plumes," Journal of Geophysical Research: Atmospheres **100**(D9), 18835–18844 (1995).

[24] Spicer, C. W., Holdren, M. W., Riggin, R. M., and Lyon, T. F., "Chemical Composition and Photochemical Reactivity of Exhaust from Aircraft Turbine Engines," Annales Geophysicae **12**(10), 944–955 (1994).

[25] Schulte, P., Schlager, H., Ziereis, H., Schumann, U., Baughcum, S. L., and Deidewig, F., "NO_x Emission Indices of Subsonic Long-range Jet Aircraft at Cuise Altitude: In situ Measurements and Predictions," Journal of Geophysical Research **102**(D17), 21431–21442 (1997).

[26] Heland, J. and Schäfer, K., "Analysis of Aircraft Exhausts with Fourier-Transform Infrared Emission Spectroscopy," Applied Optics **36**(21), 4922–4931 (1997).

[27] Anderson, B. E., Chen, G., and Blake, D. R., "Hydrocarbon Emissions from a Modern Commercial Airliner," Atmospheric Environment **40**(19), 3601–3612 (2006).

[28] Haschberger, P. and Lindermeir, E., "Spectrometric Inflight Measurement of Aircraft Exhaust Emissions: First Results of the June 1995 Campaign," Journal of Geophysical Research: Atmospheres **101**(D20), 25995–26006 (1996).

[29] Unterstrasser, S., Paoli, R., Sölch, I., Kühnlein, C., and Gerz, T., "Dimension of Aircraft Exhaust Plumes at Cruise Conditions: Effect of Wake Vortices," Atmospheric Chemistry and Physics **14**(5), 2713–2733 (2014).

[30] Clough, S. A., Iacono, M. J., and Moncet, J.-L., "Line-by-Line Calculations of Atmospheric Fluxes and Cooling Rates: Application to Water Vapor," Journal of Geophysical Research **97**(D14), 15761–15785 (1992).

[31] Clough, S. A. and Iacono, M. J., "Line-by-line Calculation of Atmospheric Fluxes and Cooling Rates 2. Application to Carbon Dioxide, Ozone, Methane, Nitrous Oxide and the Halocarbons," Journal of Geophysical Research **100**(D8), 16519–16535 (1995).

[32] COESA, "U.S. Standard Atmosphere, 1976," (1976).

[33] Rothman, L., Gordon, I., Barbe, A., Benner, D., Bernath, P., Birk, M., Boudon, V., Brown, L., Campargue, A., Champion, J.-P., Chance, K., Coudert, L., Dana, V., Devi, V., Fally, S., Flaud, J.-M., Gamache, R., Goldman, A., Jacquemart, D., Kleiner, I., Lacome, N., Lafferty, W., Mandin, J.-Y., Massie, S., Mikhailenko, S., Miller, C., Moazzen-Ahmadi, N., and Naumenko, O., "The HITRAN 2008 Molecular Spectroscopic Database," Journal of Quantitative Spectroscopy & Radiative Transfer **110**, 533–572 (2009).